Chemometrics and Intelligent Laboratory Systems 217 (2021) 104401

Contents lists available at ScienceDirect

Chemometrics and Intelligent Laboratory Systems

journal homepage: www.elsevier.com/locate/chemometrics

ATR-FTIR spectroscopy for the routine quality control of exosome isolations

Victoria Ramos-Garcia [a,1], Isabel Ten-Doménech [a,1], Alba Moreno-Giménez [a], María Gormaz [a,b], Anna Parra-Llorca [a], Alex P. Shephard [c], Pilar Sepúlveda [d], David Pérez-Guaita [e], Máximo Vento [a,b], Bernhard Lendl [f], Guillermo Quintás [g,h,*], Julia Kuligowski [a]

[a] Neonatal Research Group, Health Research Institute La Fe, Avda Fernando Abril Martorell 106, 46026, Valencia, Spain
[b] Division of Neonatology, University & Polytechnic Hospital La Fe, Avda Fernando Abril Martorell 106, 46026, Valencia, Spain
[c] Nanoview Biosciences, Malvern Hills Science Park, Geraldine Road, WR14 3SZ, Malvern, United Kingdom
[d] Regenerative Medicine and Heart Transplantation Unit, Health Research Institute Hospital La Fe, Avda Fernando Abril Martorell 106, 46026, Valencia, Spain
[e] Department of Analytical Chemistry, University of Valencia, 50 Dr. Moliner Street, 46100, Burjassot, Valencia, Spain
[f] Institute of Chemical Technologies and Analytics, Vienna University of Technology, Getreidemarkt 9/164, A 1060, Vienna, Austria
[g] Health and Biomedicine, Leitat Technological Center, Carrer de La Innovació, 2, 08225, Terrassa, Spain
[h] Analytical Unit, Health Research Institute La Fe, Avda Fernando Abril Martorell 106, 46026, Valencia, Spain

ARTICLE INFO

Keywords:
Attenuated total reflectance
Fourier transform infrared (ATR-FTIR)
Lipidomics
Exosomes
Human milk
Omics
Extracellular vesicles

ABSTRACT

Exosomes are nanosized vesicles containing specific cargos of DNA, RNA, proteins, metabolites, and intracellular and membrane lipids. Exosome isolation needs to be optimized carefully depending on the type of biofluid and tissue and the retrieved exosomes need to be characterized. The main objective of this study was to determine the feasibility of a multimodal analysis of Attenuated Total Reflectance – Fourier Transform Infrared (ATR-FTIR) spectroscopy and UPLC–QqTOF-MSMS for the development of a routine quality control tool of isolated exosomes and the rapid characterization of their lipid profiles and total protein content. Using human milk as model example, exosomes were isolated by multi-stage ultracentrifugation. After single-phase extraction, lipidomic analysis was carried out by UPLC–QqTOF-MSMS with automated MSMS-based annotation using HMDB, METLIN, LipidBlast and MSDIAL databases. The classes with the largest number of annotated features were glycerophospholipids, sphingolipids, and glycerolipids. Then, dry films of 2 μL exosomes were directly analyzed by ATR-FTIR. Multivariate analysis showed significant associations between ATR-FTIR specific regions and the concentrations of different lipid classes. Principal component analysis and Hierarchical Cluster Analysis of IR and lipidomic data showed that ATR−FTIR renders valuable qualitative descriptors of the lipid content of isolated exosomes. Total LC-MS lipid and total protein contents could also be quantified by using the area of CHs and C═O stretching bands as well as the amide I band. As a conclusion, results obtained show that multimodal analysis of ATR-FTIR and UPLC-MS data is a useful tool for the development of spectroscopic methods. ATR-FTIR provided both, qualitative and quantitative chemical descriptors of isolated exosomes, enabling a fast and direct quantification of total protein and lipid contents.

1. Introduction

Exosomes are nanosized membrane vesicles discovered in 1983, released by fusion of an organelle of the endocytic pathway, the multivesicular body, with the plasma membrane [1]. Initially, exosomes were proposed to represent cellular waste vesicles to maintain homeostasis within the cell but nowadays it is acknowledged that exosomes are associated with physiological and pathological functions [1], contributing to different aspects of physiology and disease, including intercellular communication. Besides, exosomes may have clinical applications and their use as source for diagnostic biomarkers and as drug-delivery vectors for therapeutic applications is a very active field of research [2].

Isolation techniques include differential centrifugation, ultracentrifugation, density gradient centrifugation, ultrafiltration, immunoprecipitation, and size exclusion chromatography providing different levels

* Corresponding author. Health and Biomedicine, Leitat Technological Center, Carrer de la Innovació, 2, 08225, Terrassa, Spain.
E-mail address: gquintas@leitat.org (G. Quintás).
[1] Both authors contributed equally to the study.

https://doi.org/10.1016/j.chemolab.2021.104401
Received 28 June 2021; Received in revised form 30 July 2021; Accepted 10 August 2021
Available online 18 August 2021

of recovery, purity, and sample throughput. Due to the increasing potential for the use of exosomes in clinical applications and research, there is a need to develop analytical methods to support the technical standardization of their characterization and the quality control (QC) of their isolation [3]. The characterization of exosome subpopulations and the QC of exosome isolations is a complex analytical challenge due to the diversity, heterogeneity, and complexity of their composition. Indeed, exosomes contain specific cargos of DNA or RNA including single-stranded DNA, double stranded-DNA, mitochondrial DNA, and miRNA, as well as proteins, metabolites and intracellular and membrane lipids [4], with structural and biological activity. Common techniques for their characterization include transmission electron microscopy, scanning electron microscopy, cryogenic electron microscopy, and atomic force microscopy for visualization; analysis of transmembrane proteins (i.e., tetraspanins such as CD9, CD63, and CD81) by Western blotting for identification; nanoparticle tracking analysis, asymmetric field-flow fractionation, resistance pulse sensing and protein quantification (e.g., bicinchoninic acid (BCA) assay); and the ExoView platform (NanoView Biosciences, MA, USA) for surface marker detection.

Lipid analysis of exosomes is a relatively unexplored field of research fostered by technical and methodological advances in high resolution hyphenated liquid chromatography – mass spectrometry (LC-MS). Due to their mechanisms of formation, the distribution of membrane lipids of exosomes is expected to be associated to the composition of the plasma membrane [5], including phospholipids, sphingolipids and cholesterol. Despite its sensitivity and detection range, LC-MS metabolomics requires highly skilled personal and bulky and expensive instrumentation, as well as careful sample preparation, and complex data processing and analysis steps, that limit its application for a routine QC of exosome isolations.

Attenuated Total Fourier Transform Infrared (ATR-FTIR) spectroscopy is an emerging tool in the bio-medical field for the analysis and characterization of biological samples. The technique normally relies on the fast and simple acquisition of the infrared spectrum from the untreated sample using cost-effective instrumentation and no expensive reagents or consumables. The spectra contain partially overlapped bands representative of its main components, including proteins [6], lipids [7], carbohydrates and DNA [8]. Previous results have shown that, due to its speed, simplicity, and capability for finger-printing the major components of complex samples, ATR-FTIR can be used to assess extraction procedures and sample preprocessing of biofluids in metabolomics [9]. In the field of exosome analysis, ATR-FTIR has been scarcely employed and a very limited number of applications have been proposed, including the quantification of the total protein content [10], the protein-to-lipid ratio [11], the evaluation of their isolation [12,13] as well as for the investigation of changes in the composition of saliva exosomes caused by oral cancer [14].

In this work, we aimed to assess the advantages and limitations of a multimodal analysis of ATR-FTIR spectroscopy and UPLC–MS data for the development of a routine QC tool of isolated exosomes. To this end, we employed isolated exosomes from human milk (HM) as model example and used lipidomic profiles analyzed by UPLC-QqTOF-MS, and total protein contents determined by the BCA assay as reference methodologies. To our knowledge, no study has combined ATR-FTIR and untargeted UPLC-MS-based lipidomics for the analysis of the lipid composition of isolated exosomes. Results obtained indicated that the joint analysis of IR and lipidomic information could be a powerful strategy for sensor development with potential to foster innovative cross-disciplinary research. Besides, results confirmed the capabilities of ATR-FTIR spectroscopy for a fast and direct determination of lipids and proteins, and also that this technique can be used for a rapid evaluation and characterization of the exosomes in terms of lipid composition, thus supporting its use for the QC of the exosome isolation.

2. Materials and methods

2.1. Reagents and materials

LC-MS grade acetonitrile (CH_3CN), isopropanol (IPA), and methanol (CH_3OH) were obtained from Scharlau (Barcelona, Spain); formic acid (HCOOH) (≥95%), albumin from bovine serum (≥98%), BCA Kit for Protein Determination, phosphate buffered saline (PBS) and ammonium acetate (CH_3COONH_4) (≥98%) from Sigma-Aldrich Química SL (Madrid, Spain); prostaglandin $F_{2\alpha}$-D_4 from Cayman Chemical Company (Michigan, United States); oleic acid-D_9 from Avanti Polar Lipids Inc. (Alabama, United States) and *tert*-butyl methyl ether (MTBE) (≥99%) from Fisher Scientific SL (Madrid, Spain). Ultra-pure water was generated employing a Milli-Q Integral Water Purification System from Merck Millipore (Darmstadt, Germany).

2.2. Collection of HM samples

The study was approved by the Ethics Committee for Biomedical Research of the Health Research Institute La Fe, University and Polytechnic Hospital La Fe (Valencia, Spain) with registry # 2019-289-1 and all methods were performed in accordance with relevant guidelines and regulations. Written informed consents were obtained from lactating mothers prior to sample collection and analysis of demographics and clinical information.

Ten HM samples were collected from mothers of preterm infants (<32 weeks of gestation) and term infants (>37 weeks of gestation) after establishing full enteral nutrition (i.e., stable intake of >150 ml/kg/day) using electric breast pumps following the instructions of the hospital staff. Milk was collected from full expression of one breast between 7 and 10 a.m. and preferably a minimum of 3 h after the last feed or extraction. Extracted milk was stored immediately at 4 °C and within 6 h transported to the laboratory on ice until further processing. Parameters describing the study population are shown in Table 1. In addition, two aliquots of pooled HM samples were provided by the Human Milk Bank of the University and Polytechnic Hospital La Fe.

2.3. Exosome isolation

After gentle manual shaking during 30 s, 25 mL of milk were centrifuged for removal of milk fat globules in two consecutive centrifugations at 3000×*g* for 10 min at 4 °C using an Eppendorf 5804 benchtop centrifuge with an A-4-62 rotor (Hamburg, Germany). The upper fat layer was discarded, and the supernatant was syringe-filtered (0.40 μm) prior to a third centrifugation step (3000×*g*, 10 min, 4 °C) to pellet proteins. The supernatant was collected and ultracentrifuged twice at 10000 rpm for 1 h, at 4 °C using a Hitachi CP100NX centrifuge with a Beckman Coulter 50.2 Ti rotor (Indianapolis, United States) to pellet proteins. The supernatant was syringe-filtered (0.40 μm). Then, three ultracentrifugation steps at 30000 rpm for 2 h, at 4 °C to pellet HM exosomes were performed. Between ultracentrifugation steps, supernatants were discarded, and pellets were washed with 25 mL of PBS. After the last ultracentrifugation step, supernatants were aspirated, and the isolated HM exosome pellets were suspended in 200 μL PBS and stored at −80 °C.

Table 1
Parameters of the study population.

Parameters	Median (1st-3rd quartile)
Mother's age [years]	35 (33–42)
Birth Weight [g]	1775 (1325–3078)
Gestational age [weeks]	34 ± 6 (30 ± 0–38 ± 6)
HM intake [mL/kg]	153 (150–170)
Infant's age [days]	14 (8–49)

2.4. Exosome characterization

Exosome size distribution and quantification of vesicles were analyzed using the ExoView platform (NanoView Biosciences, MA, USA). Isolated exosomes were diluted 1:25 × 10^6 in 0.22 μm pre-filtered PBS and then incubated on ExoView Human Tetraspanin chips prior to counter-staining with CD9, CD63, and CD81 fluorescent antibodies. Protein concentration was determined following the BCA Kit for Protein Determination (Sigma-Aldrich Química SL) assay based on the reduction of alkaline Cu(II) to Cu(I) by proteins in a concentration-dependent manner. BCA is a specific chromogenic reagent for Cu(I), forming a complex with an absorbance maximum at 562 nm.

2.5. ATR-FTIR spectroscopy

Infrared spectra in the 4000 to 400 cm^{-1} range were acquired using an Alpha II (Bruker Optics GmbH, Ettlingen, Germany) spectrometer equipped with a platinum-ATR with monolithic diamond measurement interface element (single reflection), a CenterGlow™ IR-source and a temperature stabilized DTGS detector with no purging system required. OPUS 8.5 software (Bruker Optics GmbH) was used to control the instrument. 2 μL of the exosome suspension were dropped onto the ATR crystal using a micropipette and then dried at room temperature for 20 s using an intermittent air stream. Spectra were collected by co-adding 32 scans with a resolution of 4 cm^{-1} using a previously recorded spectrum of air with the same instrumental conditions as background, with an acquisition time of 20 s. Between samples, the ATR interface was cleaned using a cotton swab and H_2O, IPA, and CH_3OH until recovery of the baseline signal. Spectral acquisition order was randomized but sample and spectral replicates of each exosome isolation were acquired in a row to avoid unnecessary freeze and thaw cycles that might affect their composition. All spectra were subjected to two initial quality tests. First, to guarantee that there was a significant amount of sample dried onto the ATR crystal, a minimum absorbance intensity threshold of 75 mAU was established for the amide I band. Secondly, to ensure that the contribution of water vapor to the spectra was negligible, a cut-off value of 10 was set for the ratio between the absorbance of the amide I band at 1642 cm^{-1} and the root mean square value of the mean centered absorbance in the 1820–1800 cm^{-1} interval.

2.6. Lipid extraction and LC-MS analysis

Lipids and other polar metabolites were extracted from exosomes using a single-phase extraction procedure [15] [–] [17]. 45 μL of isolated HM exosomes suspension in PBS were mixed with 5 μL of IS solution containing oleic acid-D_9 and prostaglandin $F_{2\alpha}$-D_4, 80 μM and 39 μM respectively. After 2 min of sonication, 175 μL of methanol followed by 175 μL of MTBE were added followed by mixing on a Vortex® mixer during 30 s for protein precipitation and compound extraction and sonication during 2 min to assist the release of metabolites from exosomes during extraction. After centrifugation at 4000×*g* for 15 min at 4 °C, 100 μL of supernatant containing the extracted lipids and metabolites were dried using a miVac centrifugal vacuum concentrator (Genevac LTD, Ipswich, UK) and dissolved in 100 μL of initial mobile phase (98% of mobile phase A (5:1:4 IPA:CH_3OH:H_2O 5 mM CH_3COONH_4, 0.1% v/v HCOOH) and 2% mobile phase B (99:1 IPA:H_2O 5 mM CH_3COONH_4, 0.1% v/v HCOOH)). A pooled QC sample was prepared by mixing 5 μL of each sample extract. In addition, a calibration blank (i.e., water instead of isolated exosomes) and a procedural blank (i.e., PBS supernatant from the last step of exosome isolation) were prepared, both containing IS.

Lipidomic analysis was carried out employing a 1290 Infinity HPLC system from Agilent Technologies (CA, USA) equipped with a UPLC BEH C18 column (50 × 2.1 mm, 1.7 μm, Waters, Wexford, Ireland). A binary mobile phase gradient was employed starting at 98% of mobile phase A (5:1:4 IPA:CH_3OH:H_2O 5 mM CH_3COONH_4, 0.1% v/v HCOOH) during 0.5 min followed by a linear gradient from 2 to 20% of mobile phase B (99:1 IPA:H_2O 5 mM CH_3COONH_4, 0.1% v/v HCOOH) during 3.5 min and from 20 to 95% v/v of mobile phase B in 4 min; 95% v/v of mobile phase B was maintained during 1 min; return to initial conditions was achieved in 0.25 min and were maintained for a total run time of 13 min. Column and autosampler were kept at 55 and 4 °C, respectively, the injection volume was 2 μL, and the flow rate was set to 400 μL min^{-1}. An Agilent 6550 Spectrometer iFunnel quadrupole time-of-flight (QTOF) MS system working in the ESI+ and ESI- modes was used for MS detection. Full scan MS data in the range between 70 and 1500 *m/z* were acquired at a scan frequency of 5 Hz using the following parameters: gas T, 200 °C; drying gas, 14 L min^{-1}; nebulizer, 37 psi; sheath gas T, 350 °C; sheath gas flow, 11 L min^{-1}. Mass reference standards were introduced into the source for on-the-fly automatic MS spectra recalibration during analysis via a reference sprayer valve using the 149.02332 (phthalic anhydride), 121.050873 (purine), and 922.009798 (HP-0921) *m/z* in ESI+, and 119.036 (purine) and 980.0163 (HP-0921, $[M\text{-}H + CH_3COOH]^-$) *m/z* in ESI-, as references. ESI+ and ESI- analysis were carried out in independent batches and between them, the instrument was cleaned and calibrated according to manufacturer guidelines. QCs were used to monitor the instrument performance and correct within-batch effects [18,19]. A set of 9 QCs were injected at the beginning of each batch for system conditioning and MS/MS data acquisition. MS/MS spectra were acquired using the auto MS/MS method with the following inclusion *m/z* precursor ranges: 70–200, 200–350, 350–500, 500–650, 650–800, 800–950, 950–1100, 1100–1200, and from 70 to 1200 using, in all replicates, a rate of 5 spectra/s in the extended dynamic range mode (2 GHz), a collision energy set to 20 V, an automated selection of five precursor ions per cycle and an exclusion window of 0.15 min after two consecutive selections of the same precursor. During the remaining batch sequence, a QC replicate was injected after every 5 study samples. Sample extracts were analyzed in random order. Three blank extracts were injected at the beginning and end of each batch for identifying unreliable, background, and carry-over features as described elsewhere [20].

2.7. MS data pre-processing and metabolite annotation

Peak table generation was carried out using XCMS software [21]. The *centWave* method was used for peak detection with the following parameters: mass accuracy, 20 ppm; peak width, (3,15); snthresh, 12; prefilter, (5,3000). A minimum difference in *m/z* of 7.5 mDa was selected for overlapping peaks. Intensity weighted *m/z* values of each feature were calculated using the *wMean* function. Peak limits used for integration were found through descent on the Mexican hat filtered data. Grouping before and after RT correction was carried out using the *nearest* method and 9 s as *rtCheck* argument. Finally, missing data points were filled by reintegrating the raw data files in the regions of the missing peaks using the *fillPeaks* method. The CAMERA package [22] was used for the identification of pseudospectra based on peak shape analysis, isotopic information and intensity correlation across samples [23]. Each dataset was processed with the following CAMERA functions: *xsAnnotate*, *groupFWHM*, *findIsotopes*, *groupCorr* and *findAdducts* using standard arguments. Identification and elimination of uninformative features was carried for ESI+ and ESI- data sets independently.

Metabolite annotation (Level ID: 2, putatively annotated compounds without matching to data for chemical standards acquired under the same experimental conditions) was carried out by matching experimentally acquired MS/MS spectra with the experimental HMDB, METLIN, and MSDIAL MS/MS databases in accordance with the Metabolomics Standards Initiative (MSI) reporting standards [17,24]. Metabolite annotation using LipidBlast [25] was carried out using LipiDex [26] with 0.01 Da tolerances in both MS (precursor) and MS^2 (fragment) data and the 'LipidBlast Acetate' library.

Within batch effect was removed using the non-parametric QC-Supported vector regression (SVR) correction approach employing a Radial Basis Function kernel [18,19]. The selection of the tolerance threshold (ε), the penalty term applied to margin slack values (C) and the kernel

width (γ) was carried out using a pre-selection of C and optimization of ε and γ using a grid search, leave-one-out cross validation and the root mean square error of cross validation (RMSECV) as target function. C was selected for each LC-MS feature as the median value of the intensities observed in QC replicates. The ε search range was selected based on the expected instrumental precision (4–10% of the median value of the intensities observed for the whole set of QC replicates). The γ search interval selected was [1, 10^5]. Variables with more than 2 missing values in QCs, those with RSD(QC) > 20% after QC-SVRC, and for those for which the ratio between the median peak area values in QCs and blanks was lower than 6 were classified as unreliable and removed from further analysis.

2.8. Software

UPLC-TOFMS data acquisition and manual integration was carried out employing MassHunter Workstation (version B.07.00) from Agilent. Raw data was converted into mzXML format using ProteoWizard (http://proteowizard.sourceforge.net/). Peak detection, integration, deconvolution, alignment and pseudospectra identification were carried out using XCMS and CAMERA in R 3.6.1. Metabolite annotation and data analysis were carried out in MATLAB 2017b (Mathworks Inc., Natick, MA, USA) using in-house written scripts and the PLS Toolbox 8.7 (Eigenvector Research Inc., Wenatchee, USA) as described elsewhere [17].

Statistical heterospectroscopy (SHY) [27] was employed for the joint analysis of the lipidomic and spectroscopic data acquired from the set of isolated exosome samples. SHY involved the estimation of the covariance between signal intensities measured by the two techniques across the set of samples. The SHY plot represents the correlations of IR absorbances at each wavenumber with the UPLC-MS intensities of each annotated lipid. To facilitate the extraction of information, a correlation threshold was applied. A lipid class was not represented if >50% of the correlations of its metabolites failed to reject the null hypothesis considering a 97.5% confidence level (*t*-test, unequal variances).

MATLAB scripts used datasets generated and analyzed during the current study are available in the Zenodo repository (zenodo.org/deposit/5148582).

3. Results

3.1. Characteristics of isolated HM exosomes

Fig. 1 (left) shows captured HM exosomes based on the expression of the ubiquitous tetraspanin markers CD9, CD63, and CD81 from the analysis of a representative HM exosome isolate. The marker colocalization analysis (see Fig. 1, right) shows the distribution of different tetraspanins across the membranes of the extracted HM exosomes. Most of the isolated HM exosomes expressed CD9 and CD81 while only a small fraction expressed all three tetraspanins. The employed multistep ultracentrifugation protocol allowed the extraction of HM exosomes with a median size of 61 (3 interquartile range, IQR) nm and a median number of 8×10^{14} particles mL^{-1} (3×10^{15} IQR), as determined by the ExoView platform. Protein concentrations in HM exosomes isolates determined by the BCA assay ranged between 2 and 6 g L^{-1}. Regarding the lipidomic profiles recorded from HM exosomes, Fig. 2 summarizes the main classes of the 377 features annotated in the UPLC-MS data set (208 in ESI+ and 169 in ESI-) after data pre-processing and clean-up. The classes with the largest numbers of annotated features were glycerophospholipids (50%) [glycerophosphocholines (60), glycerophosphoethanolamines (35), glycerophosphoglycerophosphoglycerols (3), glycerophosphoserines (22), glycerophosphoinositols (13), plasmenyl PCs (15), plasmenyl PEs (24), and phosphatidylinositols (11)], sphingolipids (31%) [phosphoshingolipids (71), ceramides (22), glycosphingolipids (6), hexosylceramides (17), Glc Ceramides (2)], and glycerolipids (17%) [triradylglycerols (64)].

Fig. 3 shows ATR-FTIR spectra and the first and second derivative spectra in the 3450-800 cm^{-1} range of dry residues from 2 μL of exosomes isolated from four different HM samples. The figure also shows the spectra of a blank extract with PBS bands at 1125, 1069, 978, and 851 cm^{-1}. Despite the overlap between the exosome signal and PBS bands in the 1125-850 cm^{-1} region, the use of the first or second derivative spectra enabled the resolution of overlapping spectral bands in the exosome extracts at slightly different wavenumbers (note that the minimum in a second derivative spectrum corresponds to the band apex in the raw ATR-FTIR spectrum). Spectral contributions from proteins including the amide I, II, and III were detected in exosome spectra. The amide I band governed by the stretching vibrations of C═O (70–85%) and C–N groups (10–20%) of the protein peptide backbone was detected in the 1600-1700 cm^{-1} range. The amide II band arising from in-plane N–H bending (40–60%), and C–N (18–40%) and C–C (10%) stretching vibrations was detected in the 1510-1580 cm^{-1} region. The amide III band at 1250–1350 cm^{-1} is a complex band arising from a combination of several coordinate displacements. The broad, intense band at 3285 cm^{-1} was associated to N–H stretching vibrations of peptide protein groups.

Besides, spectral contributions from carbohydrates, phosphate bands from phospholipids, DNA and RNA, and lipids were observed (see Table 2). Among them, intense bands were observed in the lipid frequency domains including the $–CH_2$ and $–CH_3$ symmetric and antisymmetric stretching (3000-2800 cm^{-1}). The characteristic C═O stretching band at 1745 cm^{-1} has been associated to the ester groups of glycerophospholipids (e.g., glycerophosphocholines, glycerophosphoethanolamines), glycerolipids (e.g., triradylglycerols), and cholesterol esters, among other lipid classes.

The differences observed in the intensity of protein and lipid bands indicate changes in the protein and lipid composition across exosome

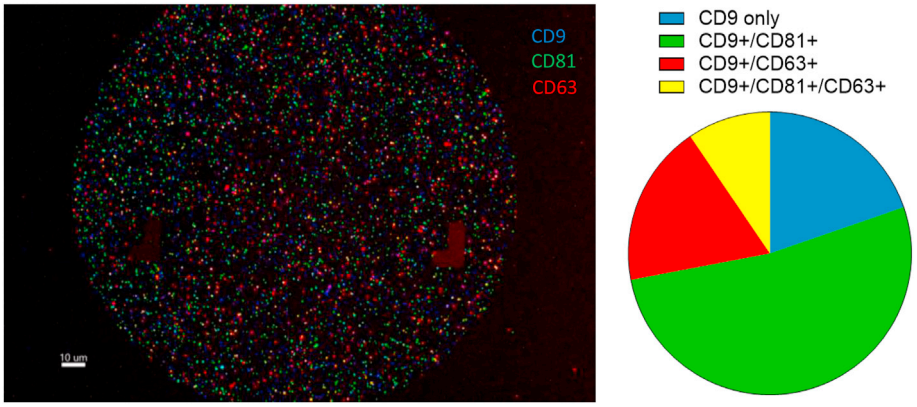

Fig. 1. Tetraspanin fluorescent staining (left) and marker colocalization analysis (right). Note: CD-9 capture.

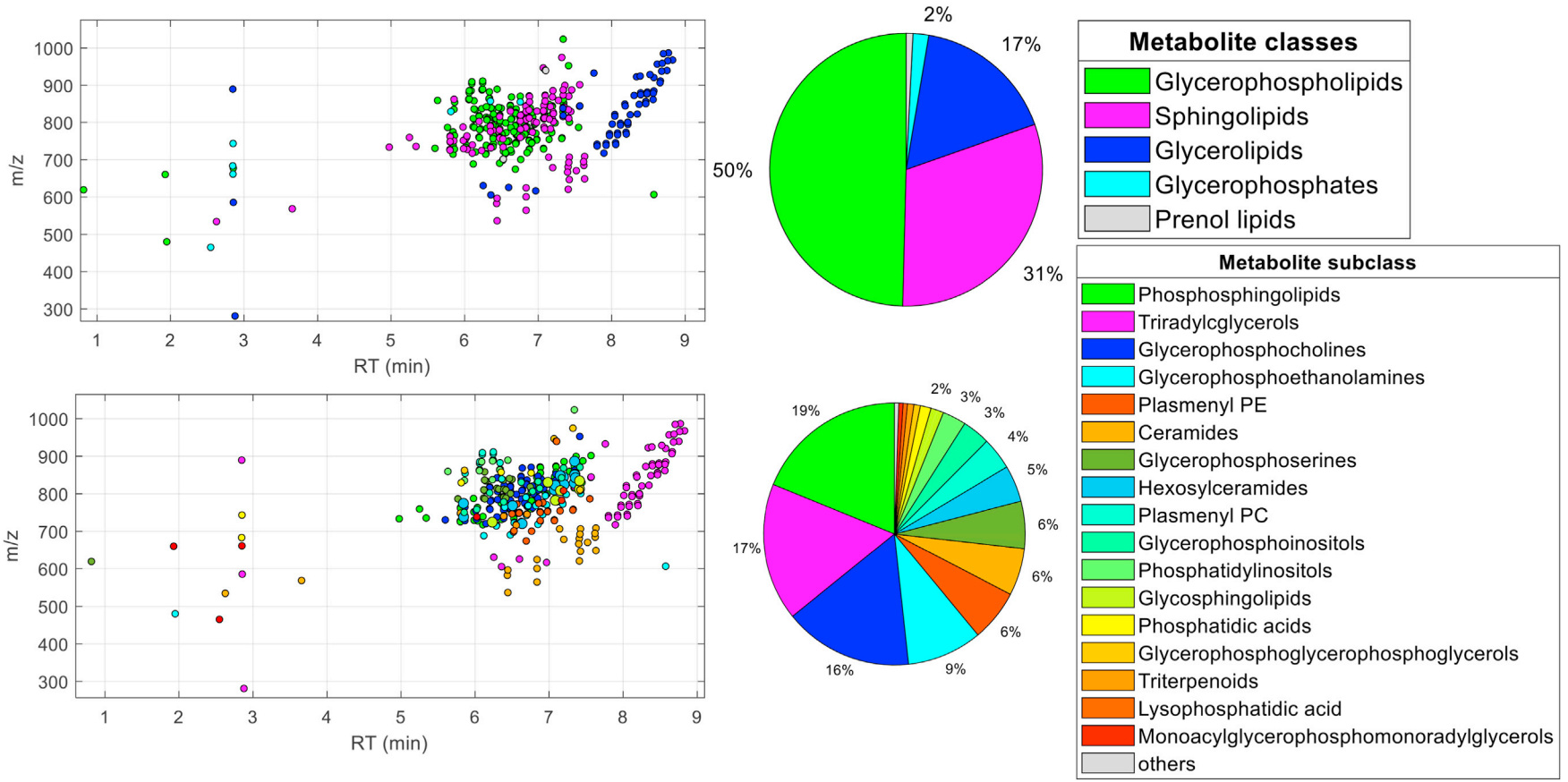

Fig. 2. Distribution of annotated UPLC–MS features detected in HM exosomes indicating their class (top) or subclass (bottom).

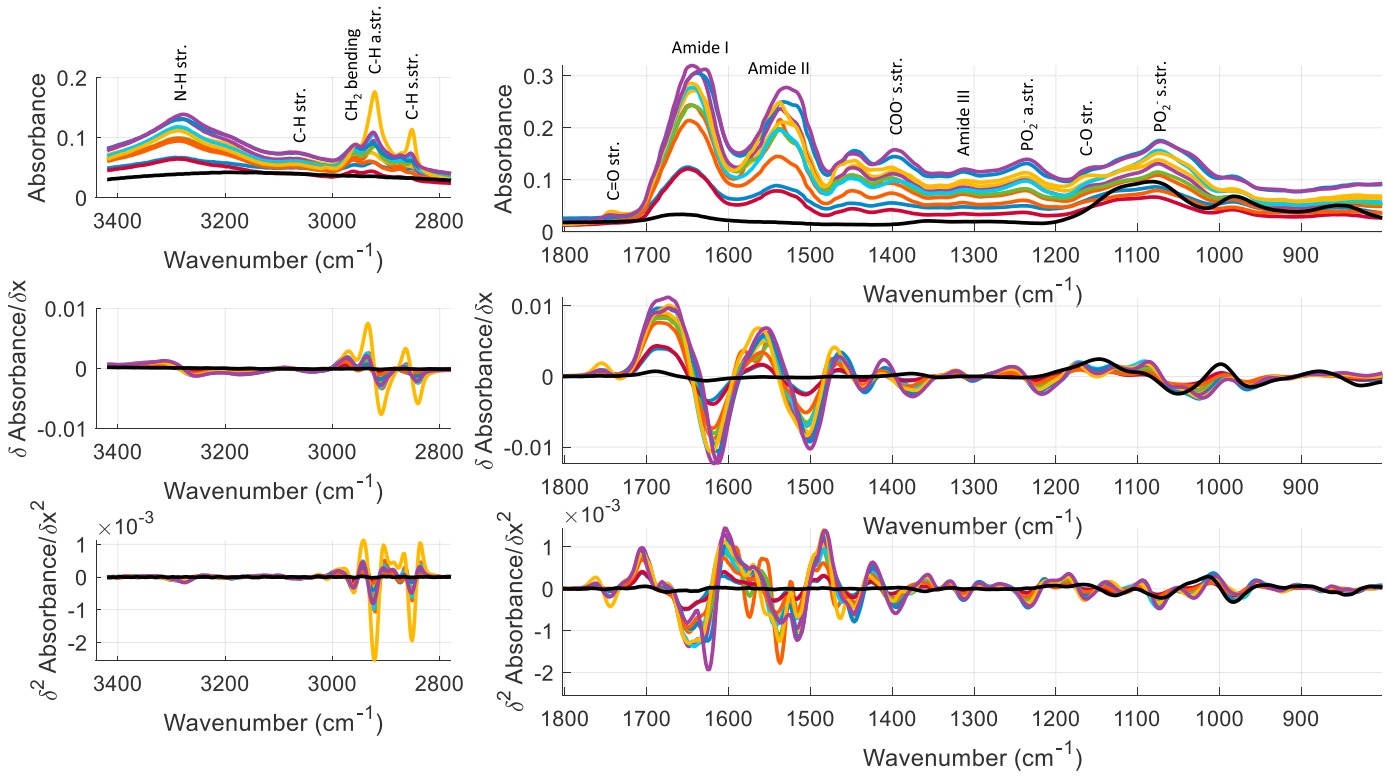

Fig. 3. ATR-FTIR raw (top), first derivative (middle) and second derivative (bottom) spectra in the 3420-2780 cm^{-1} (left) and 1800-800 cm^{-1} range (right) of dry residues obtained from 2 μL of the set of exosome extracts in PBS using a spectrum of air as background. Note: black line corresponds to a PBS blank spectrum; Colored lines: spectra of isolated exosomes from HM samples.

Table 2
Assignments of main bands observed in the ATR-FTIR spectra of HM exosomes.

Wavenumber (cm^{-1})	Spectral assignment
3285	N–H stretching (proteins)
2959	CH_3 asymmetric stretching (lipids, proteins)
2921	CH_2 anti-symmetric stretching (lipids)
2872	CH_3 symmetric stretching (lipids and proteins)
2851	CH_2 symmetric stretching (lipids)
1745	Saturated ester C=O stretch (lipids, cholesterol, phospholipids, cholesterol esters)
1646	Amide I (proteins)
1537	Amide II (proteins)
1448	CH_2 bending of lipidic acyl chains (lipids, proteins)
1402	COO− symmetric stretch (fatty acids, aminoacids)
1314	Amide III (proteins)
1236	PO_2^- antisymmetric stretch (phospholipids, nucleic acids)
1156	CO–O–C antisymmetric stretching (glycogen, nucleic acids) C–O stretching from alcohol groups (glycogen, lipids)
1080	PO_2^- symmetric stretch (phospholipids, nucleic acids)

isolations. Moreover, the marked differences in band shapes in the amide I and II region could also indicate changes in the higher order structure of proteins.

3.2. Multimodal qualitative analysis of ATR-FTIR spectra and lipidomic profiles

SHY [27] was employed to get further insight into the correlation among IR bands and UPLC-MS lipid profile. SHY enables the co-analysis of multi-source (i.e., lipidomic and spectroscopic) data sets by estimating the covariance between signal intensities measured by two techniques across the set of isolated exosome samples. Accordingly, SHY involved the calculation of a series of linear models between the ATR-FTIR absorbance for each vibrational feature and the intensities of each of the features annotated as a glycerophospholipid, sphingolipid, or glycerolipid. Results depicted in Fig. 4 show statistically significant associations (p-value<0.025) between specific overlapping regions of the raw (Fig. 4, left) and second derivative (Fig. 4, right) ATR-FTIR spectra and the different lipid classes. This result supports the potential of SHY to explore associations between lipidomic profiles and spectroscopic data and revealed relationships between the distribution of specific annotated lipid classes and the IR spectra of exosomes.

Principal component analysis (PCA) and Hierarchical Cluster Analysis (HCA) were used to identify samples with similar lipidomic profiles, using autoscaling as data preprocessing, the Pearson correlation coefficient as distance measure, and the Ward's algorithm for clustering. Fig. 5a (left) shows the scores plot of the 2 PCs model explaining 82% of the total variance in the lipidomic UPLC-MS data set. Samples were clustered mainly along PC1 in three groups including samples #7, 11, and 12 (cluster 1); #4, 5, and 9 (cluster 2); and # 1, 2, 3, 6, 8, and 10 (cluster 3). PC2 enabled the discrimination of sample 7 from 11 to 12 in cluster 1. Fig. 5a (center) depicts the scores plot of the 2 PCs model explaining 57% of the total variance in the autoscaled second-derivative ATR-FTIR data, where the samples were labeled according to the clusters selected in the lipidomic data set. Using the distances among samples as similarity criteria, results showed a similar trend: samples included in cluster 1 differ from those included in cluster 3 and were more similar to those included in cluster 2. The similarity between the trends observed in both scores plots was assessed by the Mantel test [28] which evaluated the statistical significance of the correlation between the two pairwise Euclidean distance matrices. An empirical *p*-value was estimated using a permutation test where a reference null distribution is obtained by repeatedly random shuffling the objects (here, $n = 10^4$). After each permutation, the correlation between the obtained two pairwise Euclidean distance matrices is calculated, and the *p*-value is estimated as the proportion of permuted estimates for which the absolute correlation value was equal to or greater than the correlation estimate calculated

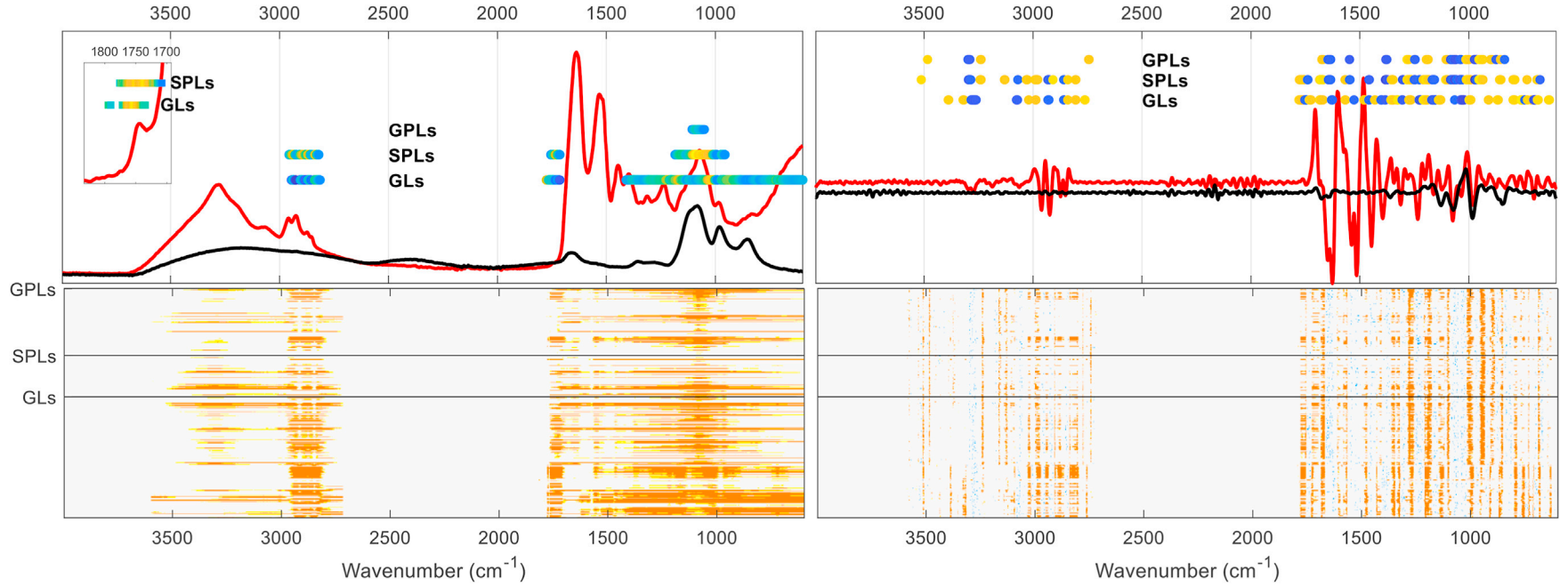

Fig. 4. Top: Median value of the correlation between annotated UPLC-MS features clustered according to their lipid classes and ATR-FTIR data (raw: left; second derivative: right) determined by SHY using the slope coefficient of a linear model. Here, only those wavenumbers for which >50% of the features of each class showed a significant correlation (p-value<0.025) are depicted. The plot overlays ATR-FTIR spectra from isolated exosomes (red) and a blank extract (black) for a better interpretation of the results. Bottom: Correlation among annotated UPLC-MS features clustered according to their lipid classes and ATR-FTIR data determined by SHY using the slope coefficient of a linear model. A correlation cutoff was applied (linear model p-value<0.025) for better visualization. Note: GPLs: glycerophospholipids; SPLs: sphingolipids, GLs: glycerolipids. Red line = HM exosome spectrum and black line = PBS blank spectrum. (For interpretation of the references to color in this figure legend, the reader is referred to the Web version of this article.)

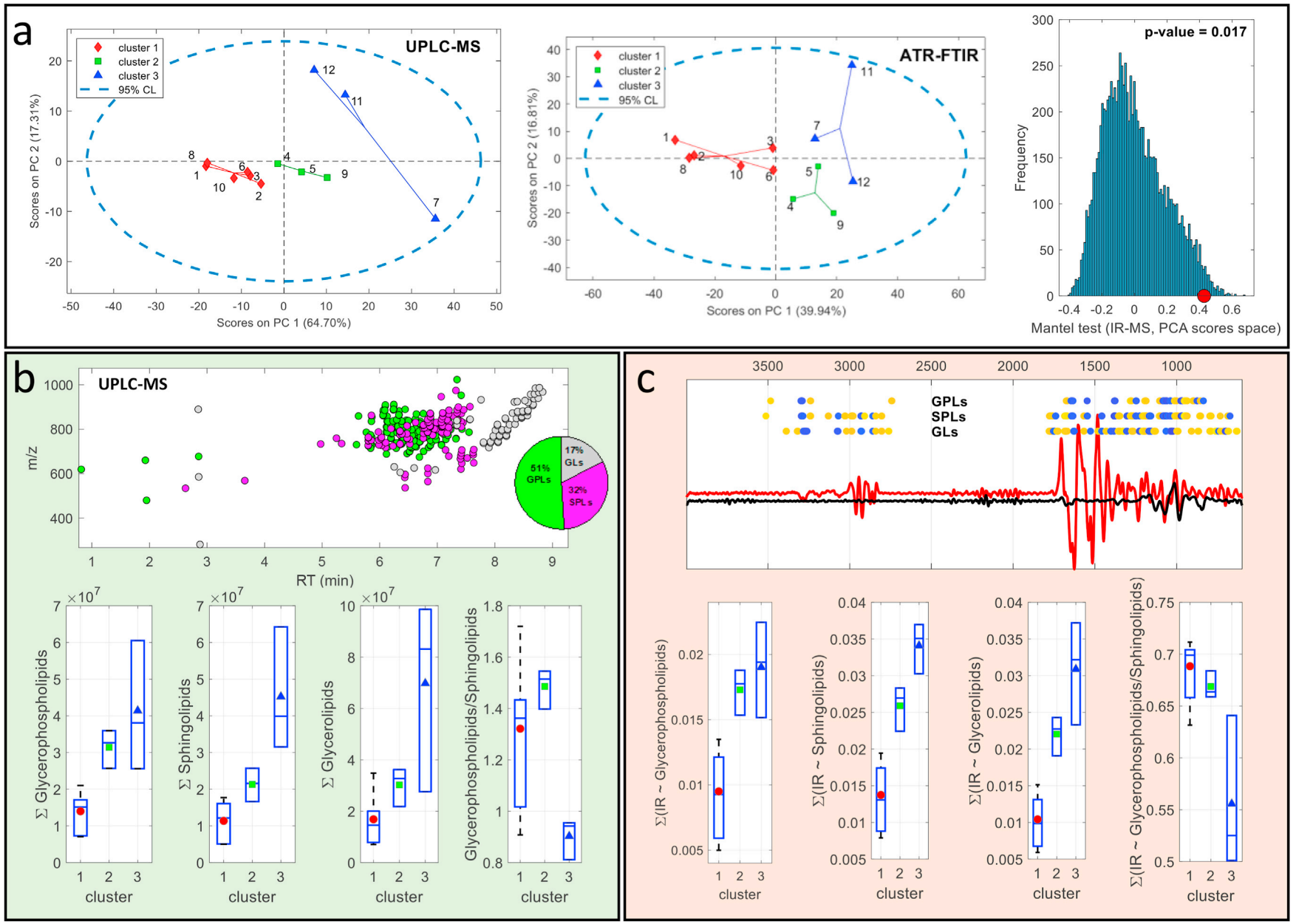

Fig. 5. a) PC1 vs PC2 scores plots from PCA of UPLC-MS lipid profiles (left), and ATR-FTIR spectra (middle). Sample classes were assigned according to the results of HCA based on UPLC-MS data. The statistical significance of the correlation between the distribution of samples in both PC1 vs PC2 scores spaces was assessed by the Mantel test (p-value<0.001) (right). b) Distribution of GLPs, GLs and SPLs features in the *m/z* vs RT space (top) and box plots showing the sum of intensities of each of these lipid classes in the three clusters (bottom). c) Second derivative ATR-FTIR spectra showing the spectral regions associated to GLs, SPLs, and GPLs (top) and sum of the intensities of the spectral regions associated to each of these lipid classes in each of the three sample clusters (bottom).
Note: GPLs: glycerophospholipids; SPLs: sphingolipids, GLs: glycerolipids.

using the original ordering. Results obtained depicted in Fig. 5a (right) (p-value<0.005) indicated a statistically significant correlation between the distribution of samples in the PCA scores spaces.

Fig. 5b shows the distribution of glycerophospholipids, sphingolipids, and glycerolipids in the RT-m/z space, as well as the boxplots representing the distributions of sum of intensities of the three classes of lipids in the three selected HCA clusters. Cluster 1 showed lower concentrations of the three lipid classes than samples included in clusters 2 and 3. Besides, although clusters 2 and 3 showed similar levels of glycerophospholipids, cluster 3 showed significantly higher relative levels of sphingolipids. Results also indicated a lower ratio of glycerophospholipids/sphingolipids in cluster 3, being cluster 2 the group of exosomes isolates with the highest ratio of glycerophospholipids/sphingolipids. Fig. 5c (top) shows the second derivative spectral regions with a statistically significant correlation with the levels of >50% of the UPLC-MS features annotated as glycerophospholipids, sphingolipids, or glycerolipids in the sample set. The boxplots representing the distributions of the sum of absolute values in the ATR-FTIR second derivative spectra associated to the three classes of lipids in the three selected HCA clusters showed a similar pattern as those found using LC-MS data.

3.3. Quantification of proteins and lipids by ATR-FTIR spectroscopy

The absorbance in the 1724-1591 cm^{-1} region showed a statistically significant correlation with the protein content determined in the isolated exosomes by the BCA assay (A=(-0.46 ± 0.34)+(1.09 ± 0.06) [protein](g/L), R^2 = 0.79, p-value<10^{-5}), in agreement with previous reports [11,29] (see Fig. 6, top left). This result suggests the use of an external calibration using a model protein (e.g., albumin) for a fast quantification of total protein content in exosomes. As shown in Fig. 6 (top, right), the exosome protein contents determined using the area of the amide I band of an external calibration line and a serial dilution of albumin standards showed a statistically significant correlation with protein concentrations determined by BCA (slope = (0.80 ± 0.05),

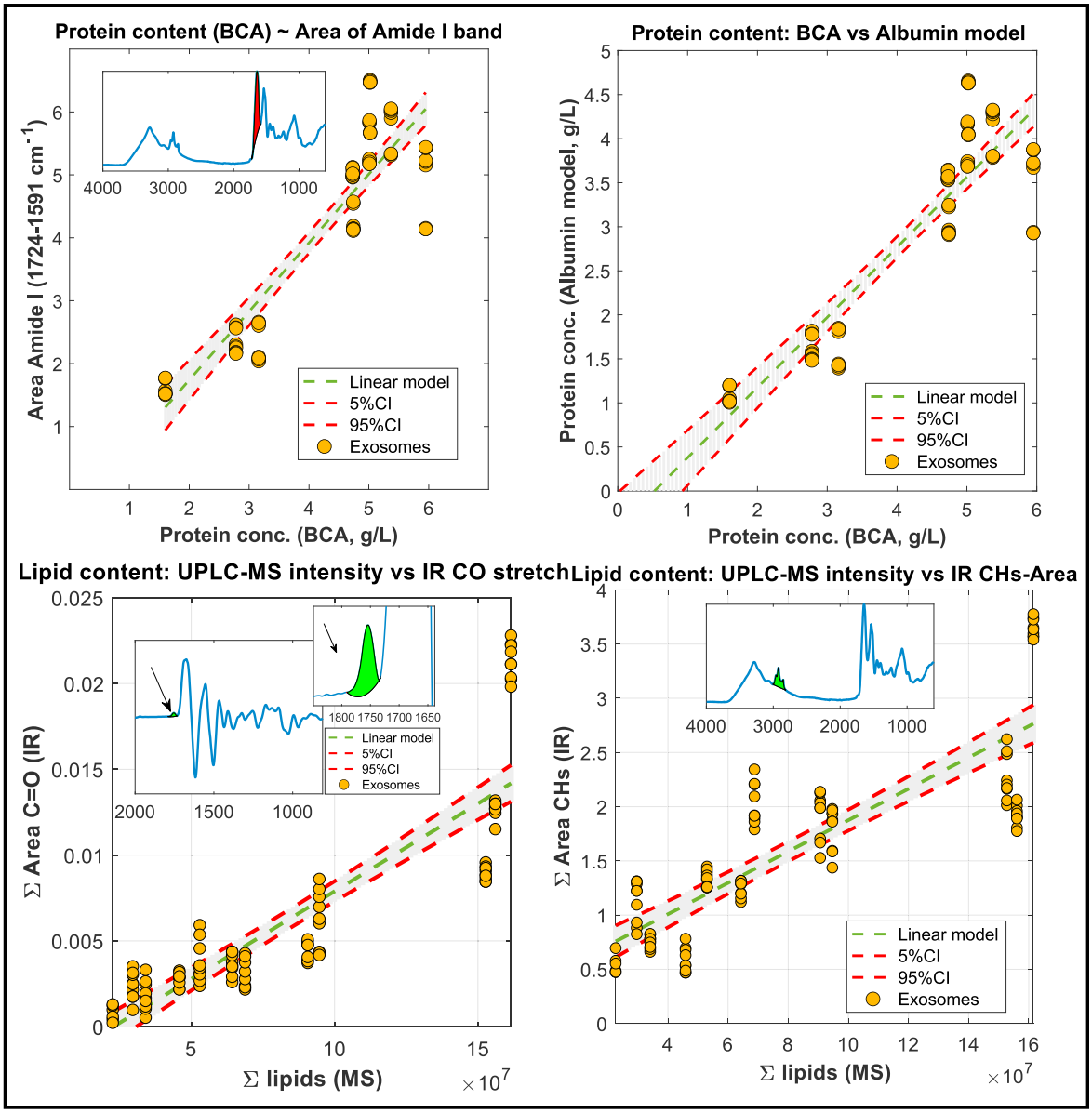

Fig. 6. Correlation between the protein content determined by the BCA assays and the amide I area in the set of isolated exosomes (top, left) and the protein content determined by BCA assays and the protein concentration determined using an external calibration line from a serial dilution of albumin solutions and amide I area (top, right). Correlation between the lipid content determined as the sum of intensities of LC-MS annotated features and the C═O (bottom, left) and CH (bottom, right) spectral area in the set of isolated exosomes.

$R^2 = 0.79$, p-value$<10^{-5}$).

The use of ATR-FTIR spectra for estimating the lipid content of exosomes was also explored. Using the sum of UPLC-MS intensities of annotated lipids as surrogate of the total lipid content in samples, the IR spectral intensity between 1790 and 1733 cm^{-1} in the first derivative spectra associated with the C═O stretching band (~1740 cm^{-1}) correlated with the lipid content (A=(-0.002 ± 0.005)+(1.02 ± 0.05) 10^{-10}[LCMS intensity](AU), $R^2 = 0.75$, p-value$<10^{-5}$) (see Fig. 6, bottom-left). Similarly, the IR spectral area in the 3000-2800 cm^{-1} range also correlated with the lipid content (A=(0.43 ± 0.09)+(1.44 ± 0.09) 10^{-8}[LCMS intensity](AU), $R^2 = 0.70$, p-value$<10^{-6}$) (see Fig. 6, bottom-right).

The repeatability of ATR-FTIR determinations is a relevant parameter for assessing its usefulness for quantitative applications. To address this concern, the RSD% observed for each wavenumber in the 3710-2717 cm^{-1} and 1840-800 cm^{-1} ranges was calculated for each sample. In this study, the set of 12 exosome samples were analyzed by replicate (n = 3), also acquiring 3 spectra/replicate. The distribution of RSD% median values obtained for each sample varied in the 3.3–11.4 RSD% range (mean value = 5 ± 1, median value = 5.4). Although these figures show acceptable reproducibility, automation of the dry-film generation for monitoring of exosome isolation would likely result in higher precision and sample throughput levels [30].

4. Discussion

We used a standard multi-step ultracentrifugation procedure for the isolation of HM exosomes from twelve HM samples. The detection of ubiquitous tetraspanins confirmed that the isolated particles are HM exosomes rather than other co-isolated contaminants. As the results from the ExoView platform, isolated exosomes showed varying particle counts, which was in good agreement with varying protein concentrations determined by the BCA assay. This reinforces the importance of quick and reproducible approaches for characterizing exosomes for routine QC. The use of a LC-MS-based lipidomic approach allowed to gain detailed insight into the composition of HM isolated exosomes (Fig. 2). The observed distribution of lipid classes agreed with the expected lipid composition of exosomes. Although their lipid profiles can be linked to their cellular origin, exosomes are bilayered proteolipids comprising mainly plasma membrane lipids (e.g., phospholipids, sphingolipids, and cholesterol) [5] enriched with bioactive cargo captured from the cytosol during the formation of the intraluminal vesicles. Previous results have observed that, compared to the cell of origin, exosome membranes are often enriched with phosphatidylserine, phosphatidylethanolamines, phosphatidylcholines, sphingolipids, and cholesterol. Besides, reported triradylglycerols could be indicative of the co-isolation of extracellular lipids during the exosome isolation, present at high concentrations in HM.

ATR-FTIR spectra showed spectral contributions from proteins, carbohydrates, phosphate bands from phospholipids, DNA and RNA, and lipids (see Fig. 3 and Table 2). Moreover, the joint analysis of LC-Ms lipidomic profiles and ATR-FTIR data (Figs. 4 and 5) showed that several spectral features were associated with different lipid classes present in HM exosomes, even though the level of detail provided by this technique is lower. However, we observed specific patterns in the ATR-FTIR spectra that were indicating the presence of the three major lipid classes (i.e., glycerophospholipids, sphingolipids, and glycerolipids) identified by LC-MS. Glycerophospholipids are glycerol-based phospholipids and spectral regions associated with >50% of glycerophospholipids included the 1100-1045 cm^{-1} region where the characteristic frequencies of the P–O–C asymmetric and symmetric stretching bands of the phosphate group can be observed. Sphingolipids are a complex family of compounds sharing a sphingoid base backbone. They were linearly correlated with ATR-FTIR absorption in the CH_2 and CH_3 symmetric and antisymmetric regions (2963-2814 cm^{-1}), C═O stretching region (1776-1708 cm^{-1}), and in the 1180-995 cm^{-1} region including characteristic frequencies associated to phosphate groups such as vC-O-PO_2^- (1060-1070 cm^{-1}) and vPO_2^- sym. (1093 cm^{-1}) [11]. Glycerolipids are also a structurally heterogeneous group of lipids composed of mono-, di-, and tri-substituted glycerols that have at least one hydrophobic chain linked to a glycerol backbone in an ester or ether linkage [31]. Spectral regions associated with this lipid class included bands at 2938–2930, 2866–2858, and 2841-2825 cm^{-1} linked to CH_2 and CH_3 symmetric and antisymmetric vibrational modes, as well as the regions 1772–1735 (C═O stretching), 1226–1141, 1053-881 cm^{-1} (C–O stretching from alcohols), and 739-698 cm^{-1}. The partial overlap between the spectral regions associated to each of the lipid classes agreed with their structural similarity, and included bands from the acyl chains, and the glycerol and phospholipid headgroups.

Furthermore, we could show that ATR-FTIR can be used for quantification. Specific lipid bands in exosomes, namely the 3000-2800 cm^{-1} range (CH stretching vibrations) and the 1790-1733 cm^{-1} (C═O stretching) showed a linear correlation with lipid contents determined by LC-MS (Fig. 6). We could also show that the same ATR-FTIR spectrum can be used for quantitation of total proteins in HM exosomes. With a simple external calibration line from serial dilutions of an albumin solution, protein concentrations determined by ATR-FTIR were found to be comparable to reference values from the BCA assay (Fig. 6). Differences observed between concentrations obtained by both techniques might be linked to the different detection principles. The amide I band is sensitive to changes in the protein structure and hence, the use of a model protein to be used as reference might bias results. On the other hand, the accuracy of the BCA assay is limited by the presence of sample reducing agents, and by the presence of cysteine, tyrosine, and tryptophan residues. Besides, the presence of reducing sugars, lipids, and phospholipids in the sample can also affect the accuracy of the BCA. Importantly, this is the first literature report on the simultaneous quantitative analysis of proteins and lipids, and qualitative lipid analysis using ATR-FTIR spectra of exosomes. In the ATR system used, the sample is deposited onto the ATR element and an IR beam is directed through an internal reflection element (IRE). Then, the evanescent wave interacts with the sample in direct contact with the IRE providing a penetration depth in the 1–3 μm range. Therefore, the repeatability of the ATR spectral acquisition depends on the distribution of the sample on top of the ATR surface, which in turn depends on the process of dry-film generation. Here, samples were manually deposited and air-dried, achieving RSD% from replicate measurements of 5 ± 1, which is within the general acceptance criteria of 15% [32].

5. Conclusions

Results obtained indicated that the joint analysis of IR and lipidomic information could be a powerful strategy for sensor development with potential to foster innovative cross-disciplinary research. Results show that ATR-FTIR spectroscopy provides both, qualitative and quantitative chemical descriptors of isolated exosomes through changes in bands associated to specific functional groups. ATR-FTIR spectroscopy enables a fast, direct quantification of total protein and lipid contents and, simultaneously, provides biochemical information useful for a routine control of changes in the relative composition of isolated exosomes in very small sample volumes (2 μL). Thus, the use of ATR-FTIR could be considered as a cost-effective alternative, to the use of standard colorimetric assays (e.g., BCA) for QC of exosome isolations. Also, whereas ATR-FTIR cannot replace the level of detailed information provided by MS in terms of specificity or sensitivity, the spectral information could be used to rapidly assess repeatability or reproducibility among exosome isolations, providing at the same time information on differences in their lipid contents.

Funding

This work was supported by the European Union's Horizon 2020

Research and Innovation Programme through the Nutrishield project (https://nutrishield-project.eu/) [Grant Agreement No 818110] and the Ayudas Intramurales 2021 para actuaciones de innovación en el ámbito de la UCIE IIS La Fe – Línea Nominativa Agencia Valenciana de Innovación [2021-071-1]. JK and ITD acknowledge support received from Instituto de Salud Carlos III (Spain) [grant numbers CP16/00034 and CD19/00176, respectively]. DPG acknowledges financial support from the Ramón y Cajal programme [grant number RYC2019-026556-I] provided by the Ministerio de Ciencia e Innovación.

The funding organizations were not involved in the collection, analysis, and interpretation of data, the writing of the report and in the decision to submit the article for publication.

CRediT authorship contribution statement

Victoria Ramos-Garcia: Formal analysis, Investigation, Methodology, Validation, Writing – review & editing. **Isabel Ten-Doménech:** Formal analysis, Investigation, Writing – review & editing. **Alba Moreno-Giménez:** Data curation, Investigation. **María Gormaz:** Data curation, Resources, Supervision. **Anna Parra-Llorca:** Data curation, Investigation. **Alex P. Shephard:** Formal analysis, Investigation, Methodology, Resources, Visualization, Writing – review & editing. **Pilar Sepúlveda:** Methodology, Investigation, Resources. **David Pérez-Guaita:** Formal analysis, Investigation, Software. **Máximo Vento:** Conceptualization, Resources. **Bernhard Lendl:** Conceptualization, Resources. **Guillermo Quintás:** Conceptualization, Data curation, Formal analysis, Investigation, Methodology, Resources, Software, Supervision, Validation, Visualization, Writing – original draft. **Julia Kuligowski:** Conceptualization, Formal analysis, Funding acquisition, Project administration, Investigation, Resources, Supervision, Validation, Visualization, Writing – review & editing.

Declaration of competing interest

The authors declare that they have no known competing financial interests or personal relationships that could have appeared to influence the work reported in this paper.

Acknowledgments

The authors are grateful to lactating mothers who agreed to participate in this study and to Amparo Ramón and Antonia Gálvez from the Human Milk Bank at the University and Polytechnic Hospital La Fe for their support and to NanoView Bioscience for technical support during exosome characterization.

References

[1] N.P. Hessvik, A. Llorente, Current knowledge on exosome biogenesis and release, Cell. Mol. Life Sci. CMLS 75 (2018) 193–208, https://doi.org/10.1007/s00018-017-2595-9.

[2] M. Zhou, S.R. Weber, Y. Zhao, H. Chen, J.M. Sundstrom, Chapter 2 - methods for exosome isolation and characterization, in: L. Edelstein, J. Smythies, P. Quesenberry, D. Noble (Eds.), Exosomes, Academic Press, 2020, pp. 23–38, https://doi.org/10.1016/B978-0-12-816053-4.00002-X.

[3] K.W. Witwer, E.I. Buzás, L.T. Bemis, A. Bora, C. Lässer, J. Lötvall, E.N.N. 't Hoen, M.G. Piper, S. Sivaraman, J. Skog, C. Théry, M.H. Wauben, F. Hochberg, Standardization of sample collection, isolation and analysis methods in extracellular vesicle research, J. Extracell. Vesicles 2 (2013) 20360, https://doi.org/10.3402/jev.v2i0.20360.

[4] Exosomes: A Rising Star in Failing Hearts, (n.d.). https://www.ncbi.nlm.nih.gov/pmc/articles/PMC5508217/(accessed January 25, 2021).

[5] T. Skotland, K. Sagini, K. Sandvig, A. Llorente, An emerging focus on lipids in extracellular vesicles, Adv. Drug Deliv. Rev. 159 (2020) 308–321, https://doi.org/10.1016/j.addr.2020.03.002.

[6] D. Perez-Guaita, Z. Richardson, P. Heraud, B. Wood, Quantification and identification of microproteinuria using ultrafiltration and ATR-FTIR spectroscopy, Anal. Chem. 92 (2020) 2409–2416, https://doi.org/10.1021/acs.analchem.9b03081.

[7] S. Yoshida, Y. Okazaki, T. Yamashita, H. Ueda, R. Ghadimi, A. Hosono, T. Tanaka, K. Kuriki, S. Suzuki, S. Tokudome, Analysis of human oral mucosa ex vivo for fatty acid compositions using Fourier-transform infrared spectroscopy, Lipids 43 (2008) 361–372, https://doi.org/10.1007/s11745-007-3147-0.

[8] B.R. Wood, The importance of hydration and DNA conformation in interpreting infrared spectra of cells and tissues, Chem. Soc. Rev. 45 (2016) 1980–1998, https://doi.org/10.1039/c5cs00511f.

[9] J. Kuligowski, D. Pérez-Guaita, J. Escobar, I. Lliso, M. de la Guardia, B. Lendl, M. Vento, G. Quintás, Infrared biospectroscopy for a fast qualitative evaluation of sample preparation in metabolomics, Talanta 127 (2014) 181–190, https://doi.org/10.1016/j.talanta.2014.04.009.

[10] V. Szentirmai, A. Wacha, C. Németh, D. Kitka, A. Rácz, K. Héberger, J. Mihály, Z. Varga, Reagent-free total protein quantification of intact extracellular vesicles by attenuated total reflection Fourier transform infrared (ATR-FTIR) spectroscopy, Anal. Bioanal. Chem. 412 (2020) 4619–4628, https://doi.org/10.1007/s00216-020-02711-8.

[11] J. Mihály, R. Deák, I.C. Szigyártó, A. Bóta, T. Beke-Somfai, Z. Varga, Characterization of extracellular vesicles by IR spectroscopy: fast and simple classification based on amide and CH stretching vibrations, Biochim. Biophys. Acta Biomembr. 1859 (2017) 459–466, https://doi.org/10.1016/j.bbamem.2016.12.005.

[12] A. Drożdż, A. Kamińska, M. Surman, A. Gonet-Surówka, R. Jach, H. Huras, M. Przybyło, E.Ł. Stępień, Low-vacuum filtration as an alternative extracellular vesicle concentration method: a comparison with ultracentrifugation and differential centrifugation, Pharmaceutics 12 (2020) 872, https://doi.org/10.3390/pharmaceutics12090872.

[13] M. Dash, K. Palaniyandi, S. Ramalingam, S. Sahabudeen, N.S. Raja, Exosomes isolated from two different cell lines using three different isolation techniques show variation in physical and molecular characteristics, Biochim. Biophys. Acta Biomembr. 1863 (2021) 183490, https://doi.org/10.1016/j.bbamem.2020.183490.

[14] A. Zlotogorski-Hurvitz, B.Z. Dekel, D. Malonek, R. Yahalom, M. Vered, FTIR-based spectrum of salivary exosomes coupled with computational-aided discriminating analysis in the diagnosis of oral cancer, J. Canc. Res. Clin. Oncol. 145 (2019) 685–694, https://doi.org/10.1007/s00432-018-02827-6.

[15] I. Ten-Doménech, V. Ramos-Garcia, J.D. Piñeiro-Ramos, M. Gormaz, A. Parra-Llorca, M. Vento, J. Kuligowski, G. Quintás, Current practice in untargeted human milk metabolomics, Metabolites 10 (2020) 43, https://doi.org/10.3390/metabo10020043.

[16] J.D. Piñeiro-Ramos, A. Parra-Llorca, I. Ten-Doménech, M. Gormaz, A. Ramón-Beltrán, M. Cernada, G. Quintás, M.C. Collado, J. Kuligowski, M. Vento, Effect of donor human milk on host-gut microbiota and metabolic interactions in preterm infants, Clin. Nutr. 40 (3) (2021) 1296–1309, https://doi.org/10.1016/j.clnu.2020.08.013, 0.

[17] I. Ten-Doménech, T. Martínez-Sena, M. Moreno-Torres, J.D. Sanjuan-Herráez, J.V. Castell, A. Parra-Llorca, M. Vento, G. Quintás, J. Kuligowski, Comparing targeted vs. Untargeted MS2 data-dependent acquisition for peak annotation in LC-MS metabolomics, Metabolites 10 (2020) 126, https://doi.org/10.3390/metabo10040126.

[18] J. Kuligowski, Á. Sánchez-Illana, D. Sanjuán-Herráez, M. Vento, G. Quintás, Intra-batch effect correction in liquid chromatography-mass spectrometry using quality control samples and support vector regression (QC-SVRC), Analyst 140 (2015) 7810–7817, https://doi.org/10.1039/c5an01638j.

[19] Á. Sánchez-Illana, D. Pérez-Guaita, D. Cuesta-García, J.D. Sanjuan-Herráez, M. Vento, J.L. Ruiz-Cerdá, G. Quintás, J. Kuligowski, Model selection for within-batch effect correction in UPLC-MS metabolomics using quality control - support vector regression, Anal. Chim. Acta 5 (2018) 62–68.

[20] T. Martínez-Sena, G. Luongo, D. Sanjuan-Herráez, J.V. Castell, M. Vento, G. Quintás, J. Kuligowski, Monitoring of system conditioning after blank injections in untargeted UPLC-MS metabolomic analysis, Sci. Rep. 9 (2019) 9822, https://doi.org/10.1038/s41598-019-46371-w.

[21] C.A. Smith, E.J. Want, G. O'Maille, R. Abagyan, G. Siuzdak, XCMS: processing mass spectrometry data for metabolite profiling using nonlinear peak alignment, matching, and identification, Anal. Chem. 78 (2006) 779–787, https://doi.org/10.1021/ac051437y.

[22] C.A. Smith, E.J. Want, G. O'Maille, R. Abagyan, G. Siuzdak, XCMS: processing mass spectrometry data for metabolite profiling using nonlinear peak alignment, matching, and identification, Anal. Chem. 78 (2006) 779–787, https://doi.org/10.1021/ac051437y.

[23] C. Kuhl, R. Tautenhahn, C. Böttcher, T.R. Larson, S. Neumann, CAMERA: an integrated strategy for compound spectra extraction and annotation of LC/MS data sets, Anal. Chem. 84 (2012) 283–289, https://doi.org/10.1021/ac202450g.

[24] R.M. Salek, C. Steinbeck, M.R. Viant, R. Goodacre, W.B. Dunn, The role of reporting standards for metabolite annotation and identification in metabolomic studies, GigaScience 2 (2013) 13, https://doi.org/10.1186/2047-217X-2-13.

[25] T. Kind, K.-H. Liu, D.Y. Lee, B. DeFelice, J.K. Meissen, O. Fiehn, LipidBlast in silico tandem mass spectrometry database for lipid identification, Nat. Methods 10 (2013) 755–758, https://doi.org/10.1038/nmeth.2551.

[26] P.D. Hutchins, J.D. Russell, J.J. Coon, LipiDex: an integrated software package for high-confidence lipid identification, Cell Syst. 6 (2018) 621–625, https://doi.org/10.1016/j.cels.2018.03.011, e5.

[27] D.J. Crockford, E. Holmes, J.C. Lindon, R.S. Plumb, S. Zirah, S.J. Bruce, P. Rainville, C.L. Stumpf, J.K. Nicholson, Statistical heterospectroscopy, an approach to the integrated analysis of NMR and UPLC-MS data Sets: application in metabonomic toxicology studies, Anal. Chem. 78 (2006) 363–371, https://doi.org/10.1021/ac051444m.

[28] N. Mantel, The detection of disease clustering and a generalized regression approach, Canc. Res. 27 (1967) 209–220.

[29] S. Navarro, D. Borchman, E. Bicknell-Brown, Lipid-protein ratios by infrared spectroscopy, Anal. Biochem. 136 (1984) 382–389, https://doi.org/10.1016/0003-2697(84)90233-1.

[30] J. Ollesch, S.L. Drees, H.M. Heise, T. Behrens, T. Brüning, K. Gerwert, FTIR spectroscopy of biofluids revisited: an automated approach to spectral biomarker identification, Analyst 138 (2013) 4092–4102, https://doi.org/10.1039/c3an00337j.

[31] R. Bittman, Glycerolipids: chemistry, in: G.C.K. Roberts (Ed.), Encycl. Biophys., Springer, Berlin, Heidelberg, 2013, pp. 907–914, https://doi.org/10.1007/978-3-642-16712-6_527.

[32] Food and Drug Administration (FDA), Guidance for Industry: Bioanalytical Method Validation. Food and Drug Administration, Center for Drug Evaluation and Research, Center for Veterinary Medicine, 2018, p. 44.